THE JOURNAL OF BIOLOGICAL CHEMISTRY
Vol. 280, No. 19, Issue of May 13, pp. 18891–18898, 2005
Printed in U.S.A.

A Structural Basis for 14-3-3σ Functional Specificity* ♦

Received for publication, January 26, 2005, and in revised form, February 22, 2005
Published, JBC Papers in Press, February 24, 2005, DOI 10.1074/jbc.M500982200

Erik W. Wilker‡, Robert A. Grant‡, Stephen C. Artim, and Michael B. Yaffe§

From the Center for Cancer Research, Department of Biology and Division of Biological Engineering, Massachsuetts Institute of Technology, Cambridge, Massachusetts 02139

The 14-3-3 family of proteins includes seven isotypes in mammalian cells that play numerous diverse roles in intracellular signaling. Most 14-3-3 proteins form homodimers and mixed heterodimers between different isotypes, with overlapping roles in ligand binding. In contrast, one mammalian isoform, 14-3-3σ, expressed primarily in epithelial cells, appears to play a unique role in the cellular response to DNA damage and in human oncogenesis. The biological and structural basis for these 14-3-3σ-specific functions is unknown. We demonstrate that endogenous 14-3-3σ preferentially forms homodimers in cells. We have solved the x-ray crystal structure of 14-3-3σ bound to an optimal phosphopeptide ligand at 2.4 Å resolution. The structure reveals the presence of stabilizing ring-ring and salt bridge interactions unique to the 14-3-3σ homodimer structure and potentially destabilizing electrostatic interactions between subunits in 14-3-3σ-containing heterodimers, rationalizing preferential homodimerization of 14-3-3σ *in vivo*. The interaction of the phosphopeptide with 14-3-3 reveals a conserved mechanism for phospho-dependent ligand binding, implying that the phosphopeptide binding cleft is not the critical determinant of the unique biological properties of 14-3-3σ. Instead, the structure suggests a second ligand binding site involved in 14-3-3σ-specific ligand discrimination. We have confirmed this by site-directed mutagenesis of three σ-specific residues that uniquely define this site. Mutation of these residues to the alternative sequence that is absolutely conserved in all other 14-3-3 isotypes confers upon 14-3-3σ the ability to bind to Cdc25C, a ligand that is known to bind to other 14-3-3 proteins but not to σ.

14-3-3 denotes a family of ~30-kDa dimeric proteins found in all eukaryotic cells (1–5). This family of highly conserved proteins consists of seven distinct gene products in human cells (β, γ, ϵ, η, σ, τ, and ζ) as well as a variety of post-translationally modified forms (6–9). To the extent that it has been investigated, broad heterodimerization has generally been observed between the different 14-3-3 isoforms (10, 11). In addition, all 14-3-3 proteins bind to common phosphoserine/phosphothreonine-containing peptide motifs corresponding to Mode-1 (RS*X*-pS*X*P) or Mode-2 (R*XXX*pS*X*P) sequences (12).

14-3-3 proteins participate in a wide variety of signal transduction processes including Ras-Raf-mediated activation of the mitogen-activated protein kinase pathway, regulation of apoptosis, adhesion-dependent integrin signaling, and cell cycle control in response to genotoxic stress (1–5). All of these processes appear to involve multiple 14-3-3 isotypes. Although some isotype-specific differences in signaling clearly exist, the molecular basis for these differences remain obscure and difficult to rationalize given the strong sequence conservation and broad heterodimerization observed among the individual 14-3-3 proteins.

We have been particularly interested in understanding the roles of different 14-3-3 proteins in cell proliferation, cell cycle control, and human tumorigenesis (5, 13, 14). In epithelial cells, one particular 14-3-3 isoform, 14-3-3σ, appears to play a particularly important role in this regard. Hermeking *et al.* (15) demonstrated that 14-3-3σ was a major p53 response gene in HCT116 colon carcinoma cells following exposure to DNA damaging agents and suggested a role for 14-3-3σ in G_2/M checkpoint function. Chan *et al.* (16) found that 14-3-3σ−/− HCT116 cells were unable to maintain the G_2/M checkpoint arrest following exposure to adriamycin and subsequently died by mitotic catastrophe. One well established function of 14-3-3 in negatively regulating M-phase entry involves functional sequestration of the mitotic promoting phosphatase Cdc25C (17–20). Intriguingly, however, 14-3-3σ does not bind to Cdc25C (16, 21), suggesting that alternative σ-specific ligands, whose identities remain unknown, must also play important roles in controlling progression from G_2 into M by some Cdc25C-independent mechanism.

Given the importance of 14-3-3σ in mitotic regulation, it is paradoxical that many different types of epithelial cancers have recently been found to down-regulate 14-3-3σ expression at the mRNA and protein level, either through promoter methylation and gene silencing (22–26) or through up-regulation of a specific E3 ubiquitin ligase that targets 14-3-3σ for destruction (27). This may be related to an alternative function of 14-3-3σ in promoting cell senescence, although to date this has only been demonstrated in human keratinocytes (28).

Why is 14-3-3σ apparently unique among the mammalian isoforms? What is structural basis for the distinct function of σ and its ligand discrimination? Why are 14-3-3σ effects not diluted out through heterodimerization with other 14-3-3 isotypes? This study was designed to investigate structural differences between 14-3-3σ and other 14-3-3 family members in an attempt to provide a molecular rationalization for some of these aspects of σ-specific function.

* This work was supported by postdoctoral fellowships from the Anna Fuller Fund and the National Institutes of Health (NIH) (to E. W. W.), by the David H. Koch Cancer Research Fund, by NIH Grants GM60594 and GM68762, and by a Burroughs-Wellcome Career Development Award (to M. B. Y.). The costs of publication of this article were defrayed in part by the payment of page charges. This article must therefore be hereby marked "*advertisement*" in accordance with 18 U.S.C. Section 1734 solely to indicate this fact.

♦ This article was selected as a Paper of the Week.

The atomic coordinates and structure factors (code 1YWT) have been deposited in the Protein Data Bank, Research Collaboratory for Structural Bioinformatics, Rutgers University, New Brunswick, NJ (http://www.rcsb.org/).

‡ These authors contributed equally to this work.

§ To whom correspondence should be addressed: MIT Center for Cancer Research, 77 Massachusetts Ave., E18-580, Cambridge, MA 02139. Tel.: 617-452-2103; Fax: 617-452-4978; E-mail: myaffe@mit.edu.

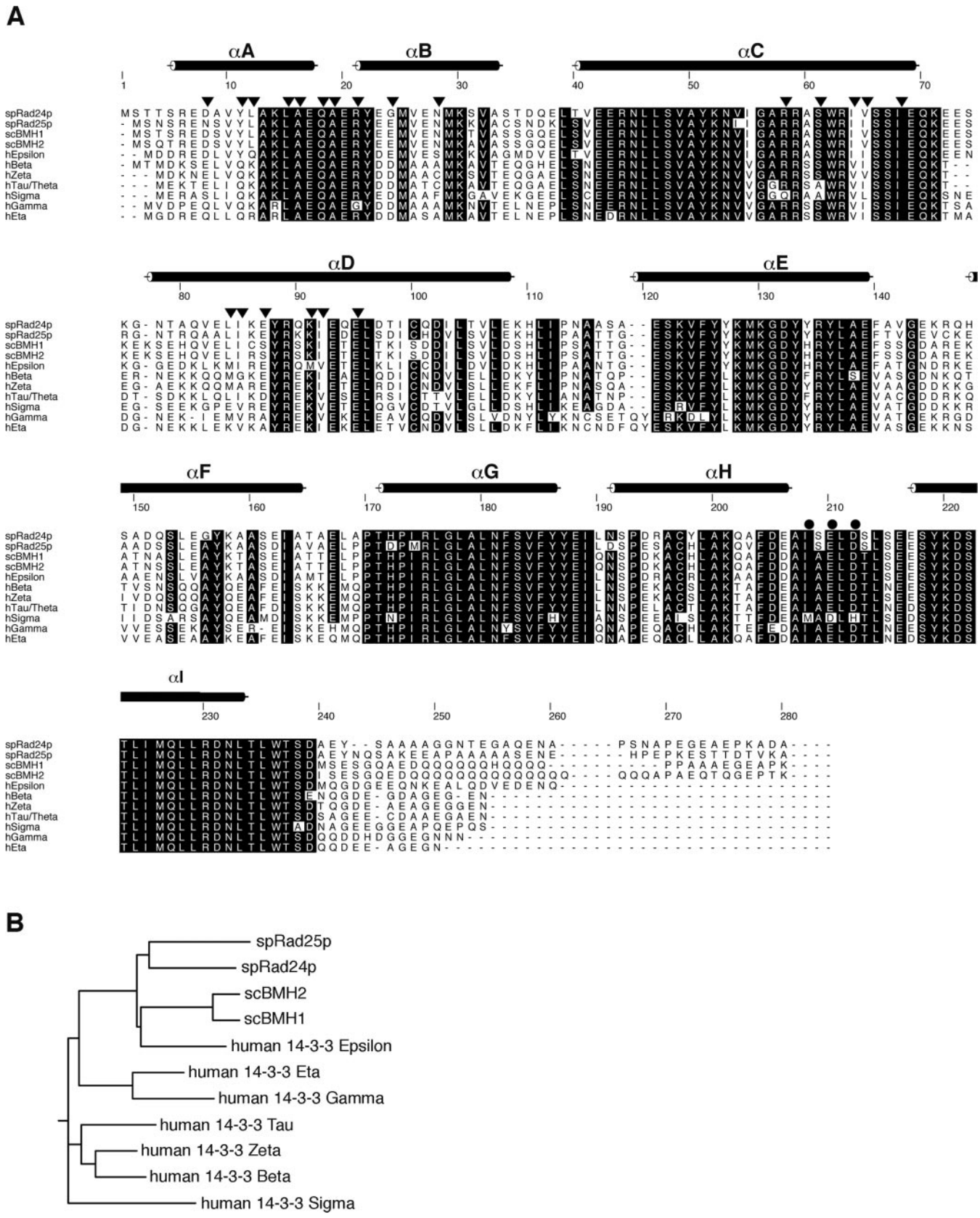

FIG. 1. **Sequence conservation among 14-3-3 proteins.** *A*, sequence alignment. ClustalW-based sequence alignment of all human (*h*) 14-3-3 isotypes, the 14-3-3 proteins from the budding yeast *Saccharomyces cerevisiae* (*sc*), and the fission yeast *Saccharomyces pombe* (*sp*). *Inverted triangles* demarcate residues at the dimerization interface; *solid circles* indicate a critical three-amino acid alteration in 14-3-3σ involved in substrate discrimination. *B*, 14-3-3 cladogram. A rooted phylogenetic tree of the sequences in *A* generated using PHYLIP (40) reveals that 14-3-3σ is evolutionarily distinct from clades encompassing all other 14-3-3 isotypes.

MATERIALS AND METHODS

Construct Design and Recombinant Protein Expression—The pCDNA3.1 vector for mammalian expression of HA[1]-tagged 14-3-3σ has been described previously (21). The HA-tagged 14-3-3σ M202I,D204E, H206D triple mutant was generated using site-directed PCR mutagenesis with HA-14-3-3σ pCDNA3.1 as a template. The following two primer sets were used: AGGGAGACCCAAGCTTACCAT (forward-1) and GAGGGTGTCCAGTTCAGCAATGGCCTC (reverse-1) and GAGGCCATTGCTGAACTGGACACCCTC (forward-2) and TGATTAGGGTGATGGTTCACG (reverse-2) to create a PCR product that was ligated into the HindIII/XhoI sites in the pcDNA3.1 expression vector using Roche's Rapid DNA ligation kit (Roche Applied Science). A vector for low level mammalian expression of 2×FLAG-tagged 14-3-3σ was generated by first inserting a Kozak sequence and 2×FLAG epitope into the BamHI/EcoRI sites of pCDNA3.1+ using the following oligonucleotides: 5′-GATCCGCCACCATGGATTACAAGGATGACGACGATAAGGATTACAAGGATGACGACGATAAGG-3′ and 5′-AATTCCTTATCGTCGTCATCCTTGTAATCCTTATCGTCGTCATCCTGTAATCCATGGTGGCG-3′. 14-3-3σ was then PCR amplified with EcoRI/XhoI compatible ends and subcloned into the EcoRI/XhoI sites of the pCDNA3.1 + 2×FLAG vector. The final 2×FLAG-14-3-3σ cassette was then subcloned into the BamHI/EcoRV sites of the tetracycline-inducible vector pTRE (BD Biosciences). Low level expression of 2×FLAG-14-3-3σ was obtained by culturing transfected cells in media lacking tetracycline.

pGEX vectors for bacterial expression of glutathione *S*-transferase-tagged 14-3-3σ, -β, -γ, -ϵ, and -ζ have been described previously (12). A bacterial expression vector for production of recombinant untagged 14-3-3σ for use in crystallization studies was generated by PCR amplifying 14-3-3σ from pGEX-14-3-3σ with NcoI/HindIII compatible ends and subcloning the PCR product into the NcoI/HindIII sites of pKK233-2. All vector constructs were transformed into DH5α *Escherichia coli*. Following colony selection, plasmid DNA was prepared (Qiagen) and the sequence verified by dideoxy sequencing.

Bacterial expression of recombinant proteins was performed by transforming BL21(DE3) *E. coli* with the appropriate plasmids, followed by growth in LB medium containing ampicillin. Cultures were induced at an A_{600} of 0.6–0.8 by addition of isopropyl β-D-thiogalactopyranoside to a final concentration of 0.4 mM followed by growth for 4 h at 37 °C prior to cell harvesting by centrifugation.

Tissue Culture and Mammalian Cell Transfections—U20S cells (passage 12, ATCC) were cultured in Dulbecco's modified Eagle's medium/HEPES medium supplemented with 10% fetal calf serum, glutamine, and penicillin/streptomycin in 10-cm^2 culture dishes. The HA- and 2×FLAG-tagged 14-3-3 constructs (4 μg) were transfected into ~50% confluent U2OS cells using FuGENE 6 transfection reagent as recommended by the manufacturer. Where indicated, cells were treated with 10 Gy of ionizing radiation 24 h following transfection.

Preparation of Whole Cell Lysates, Immunoprecipitation, and Western Blot Analysis—Whole cell lysates were prepared by scraping U2OS cells into modified radioimmune precipitation assay buffer (50 mM Tris-HCl, pH 7.6, 150 mM NaCl, 1 mM EDTA, 1% Nonidet P-40, containing 1 mM phenylmethylsulfonyl fluoride, 1 μg/ml aprotinin, 1 μg/ml leupeptin, 1 μg/ml pepstatin, 1 mM Na_3VO_4, 20 nM microcystin LR, 5 nM okadaic acid, 2 μM cantharidin, 0.00073% *p*-bromotetramisole, 10 μM E64, and 1 mM AEBSF) and pushed through a syringe equipped with a 30-gauge needle three times. Lysates were incubated for 15 min at 4 °C, centrifuged at 12,000 × *g* for 15 min at 4 °C, and the supernatants recovered. Protein concentration was measured using the Bio-Rad protein assay kit.

Immunoprecipitations were performed using 1 mg of whole cell lysates and 4 μg of the appropriate antibodies overnight at 4 °C. Following binding to protein-A-Sepharose beads for 1 h at 4 °C, the immunoprecipitates were washed three times with modified radioimmune precipitation assay buffer, suspended in Laemmli sample buffer, resolved on SDS-PAGE gels, and transferred to polyvinylidene difluoride membranes. The membranes were blocked for 1 h at 4 °C using 5% nonfat dry milk (Bio-Rad) in phosphate-buffered saline containing 0.05% Tween 20, followed by incubation for 1–2 h at room temperature or overnight at 4 °C with mouse monoclonal antibodies specific for the HA epitope (clone 12CA5; Roche Applied Science) or 14-3-3σ (clone CS-112 (29)) or with rabbit or goat polyclonal antibodies against 14-3-3β (C-20), c-Raf-1 (C-12), and Cdc25C (C-19) or an antibody that recognizes all 14-3-3 isotypes (K-19), all from Santa Cruz Biotechnology (Santa Cruz, CA). Primary antibodies were used at dilutions between 1:1000 and 1:2500. Blots were washed three times for 15 min each with phosphate-buffered saline containing 0.05% Tween 20, followed by incubation with the appropriate horseradish peroxidase-conjugated secondary antibodies at 1:2500–1:5000 dilution for 60 min at room temperature. Following washing, immunoreactive bands were visualized by enhanced chemiluminescence (PerkinElmer Life Sciences) and the blots exposed to x-ray film (Eastman Kodak Co.).

Two-dimensional Gel Electrophoresis—For two-dimensional electrophoresis, immunoprecipitations from whole cell extracts were suspended in 100 μl of focusing buffer (8 M urea, 2 M thiourea, 4% CHAPS, 15 mg/ml DTT, 2% ampholytes) cup-loaded onto prerehydrated 7-cm IPG strips (pH 4–7, all strips from the same lot), and subjected to isoelectric focusing for 15 min at 100 V, 15 min at 200 V, 30 min at 500 V, 1 h at 1000 V, and 6 h at 3500 V using an IPGphor isoelectric focusing

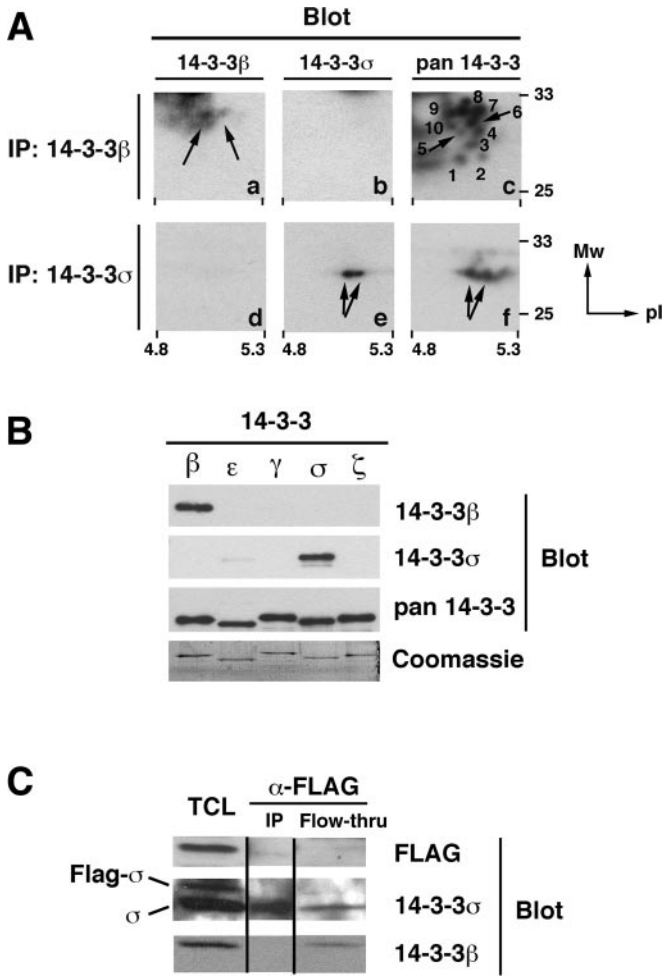

FIG. 2. **14-3-3σ primarily forms homodimers in cells.** *A*, homodimerization revealed by two-dimensional gel Western blot analysis. U2OS whole cell lysates were immunoprecipitated with antibodies against 14-3-3β (*panels a–c*) or 14-3-3σ (*panels d–f*) and analyzed for co-associated 14-3-3 isotypes by two-dimensional gel electrophoresis and Western blotting. The two spots observed for 14-3-3β and -σ indicate post-translational modifications. A fraction of 14-3-3β is known to be phosphorylated on Ser-185 (6); the post-translational modification of 14-3-3σ is not known. *B*, antibody controls. Bacterial lysates containing recombinant glutathione *S*-transferase-14-3-3 fusion proteins were separated by SDS-PAGE and blotted with the antibodies used in *A*. A duplicate gel was stained with Coomassie Blue (*lower panel*). *C*, homodimerization confirmed by epitope tagging. U2OS cells were transfected with 2×FLAG-tagged 14-3-3σ. Total cell lysates (*TCL*) were prepared 24 h later, incubated with bead-immobilized anti-FLAG antibodies, and the immunoprecipitated proteins (*IP*) released under nonreducing conditions to minimize interfering signals from the antibody light chain. Under these conditions, the 2×FLAG-tagged 14-3-3σ remained bound to the antibody-immobilized beads. Total cell lysate and immunoprecipitated protein samples, along with unbound material (*Flow-thru*) in the anti-FLAG-depleted lysates, were analyzed by blotting with the indicated antibodies.

[1] The abbreviations used are: HA, hemagglutinin; AEBSF, 4-(2-aminoethyl)benzenesulfonyl fluoride; CHAPS, 3-[(3-cholamidopropyl)dimethylammonio]-1-propanesulfonic acid; DTT, dithiothreitol.

TABLE I
Crystallographic data and refinement statistics

Space group:	$C222_1$; a = 56.2 Å, b = 137.1 Å, c = 155.3 Å
Asymmetric unit:	14-3-3 dimer with a phosphopeptide bound to each monomer
Data collection	
Wavelength (Å)	0.97949
Resolution (Å)	40–2.4
R_{sym} [a]	0.095 (0.652)[b]
Completeness (%)	99.2 (99.3)
Unique *hkl* reflections	24,430
Redundancy (-fold)	15.1 (13.5)
Average I/σ	30.7 (5.4)
Refinement	
$hkl\|F > 0\|$ reflections	22,712
hkl (test set)	2241
R_{work} (%)[c]	23.3
R_{free} (%)[d]	28.3
	3656 protein atoms, 55 solvent atoms, 1 calcium ion
Root mean square deviations	
Bonds (Å)	0.007
Angles (degrees)	1.07

[a] $R_{sym} = \Sigma_h\Sigma_j|I_j(h) - \langle I(h)\rangle|/\Sigma_h\Sigma_j\langle I(h)\rangle$, where $I_j(h)$ is the jth reflection of index h and $\langle I\rangle$ is the average intensity of all observations of $I(h)$.
[b] Values in parentheses are for the highest resolution bin (2.49–2.40Å).
[c] $R_{work} = \Sigma_h|F_{obs}(h) - F_{calc}(h)|/\Sigma_h|F_{obs}(h)|$, calculated over the 90% of the data in the working set.
[d] R_{free} is equivalent to R_{work} except calculated over the 10% of the data assigned to the test set.

system device (Amersham Biosciences). Strips were washed in re-equilibration buffer (50 mM Tris-HCl, pH 8.8, 6 M urea, 30% glycerol, 2% SDS) in the presence of 20 mg/ml dithiothreitol for 10 min and then in the presence of 25 mg/ml iodoacetamide for 10 min to irreversibly modify all cysteine residues. The strips were then loaded onto 12% SDS-PAGE gels and electrophoresed at 120 V for 1 h. Gels were transferred onto polyvinylidene difluoride membranes and used for Western blot analyses using the appropriate antibodies in conjunction with enhanced chemiluminescence detection.

14-3-3σ Purification, Crystallization, and Structure Solution—Pellets of bacteria expressing untagged 14-3-3σ corresponding to 3 liters of culture were suspended in 200 ml of lysis buffer (50 mM Tris-HCl pH 8.0, 300 mM NaCl, 2 mM DTT, 1 mM AEBSF) and lysed by sonication. The lysate was clarified by centrifugation, diluted to 100 mM NaCl with dilution buffer (50 mM Tris-HCl, pH 8.0, 2 mM DTT), and loaded onto a Q-Sepharose column equilibrated with buffer QA (100 mM Tris-HCl, pH 8.0, 50 mM NaCl, 2 mM DTT). The column was washed extensively in the same buffer and the protein then eluted with a 100–500 mM NaCl gradient. Fractions containing 14-3-3σ, determined by SDS-PAGE analysis, were pooled and dialyzed against gel filtration buffer (50 mM Tris-HCl, pH 8.0, 200 mM NaCl, 2 mM DTT) and concentrated by ultracentrifugation to ~2 ml for loading onto a Superdex-75 gel filtration column. Appropriate fractions from the gel filtration column were dialyzed into buffer HA (10 mM Tris-HCl, pH 8.0, 10 mM NaCl, 2 mM DTT) and loaded onto a hydroxyapatite column equilibrated with buffer HA. Protein was eluted with a linear gradient from buffer HA to buffer HB (250 mM sodium phosphate, pH 7.0, 50 mM NaCl, 2 mM DTT). Purified 14-3-3σ (~8 mg) was dialyzed into 10 mM Tris-HCl, pH 8.0, 10 mM NaCl, concentrated to ~10 mg/ml by ultrafiltration, divided into 250-μg aliquots, and flash-frozen in liquid nitrogen.

An optimal mode-1 phosphopeptide was synthesized using *N*-α-Fmoc (*N*-(9-fluorenyl)methoxycarbonyl)-protected amino acids with standard BOP/HOBt coupling chemistry and purified by reverse phase high performance liquid chromatography. Protein-peptide complexes were prepared at 5 mg/ml protein by combining freshly thawed protein stock with a 2-fold molar excess of phosphopeptide and dilution with water. Crystals were grown at 18 °C by vapor diffusion in hanging drops over 1–2 weeks. 1–2 μl of complex was mixed with an equal volume of well solutions containing 50 mM HEPES, pH 7.0, 6–10% polyethylene glycol 3350, 100–150 mM NaF, and 40 mM $CaCl_2$. Crystals were frozen in liquid nitrogen after a brief soak in synthetic mother liquor containing 15% glycerol, which was made by adding a 50% solution of glycerol in well solution directly to the hanging drop.

Crystals were screened on a Rigaku rotating anode source with Yale mirror optics and a R-AXIS IV detector. A 2.4 Å resolution data set was collected at 100 K using the NE-CAT 8BM beamline at the Advanced Photon Source, Argonne National Laboratory (Chicago, IL). The space group of the crystals was $C222_1$, with a single 14-3-3 dimer and its two bound peptides in the asymmetric unit. The data were indexed, integrated, and scaled using HKL2000 (30), and the structure was solved by molecular replacement using AmoRe (31) with the 14-3-3ζ dimer (with the peptide removed) from the 14-3-3ζ-mode-2 peptide complex structure (Protein Data Bank code 1QJA) as the search model. Phase refinement was performed using CNS (32). The structure was built using the O program (33), and figures were prepared using PyMOL (www.pymol.org). Coordinates have been deposited in the Protein Data Bank as 1YWT.

RESULTS AND DISCUSSION

A comparison of the sequence of 14-3-3σ with that of other human 14-3-3 isotypes, as well as with those in the evolutionarily distant budding and fission yeast (Fig. 1*A*), reveals many regions of considerable sequence conservation. Despite this strong global sequence preservation, there are a number of short regions in 14-3-3σ that differ in general from those in other 14-3-3 proteins. A particularly striking example is a unique 3 amino acid substitution in the αH-αI linker. Phylogenetic analysis (Fig. 1*B*) reveals that σ is the most divergent of all 14-3-3 proteins, consistent with its apparently unique function *in vivo*. All other 14-3-3 proteins can be clustered into three major clades, one containing 14-3-3ε together with the yeast isoforms, a second clade containing the η and γ isoforms, and a third clade containing the τ, β, and ζ isoforms. The structure of 14-3-3σ gene on chromosome 1, together with its complete lack of introns (a feature unique to σ), support a hypothesis that 14-3-3σ may represent a functional retrotransposed gene.

Given the propensity of 14-3-3 proteins to form both homodimers and mixed heterodimers with other 14-3-3 isotypes (10, 11), what accounts for the functional specificity of 14-3-3σ revealed by mammalian genetic experiments (16)? To address this question, the extent of 14-3-3σ homo- *versus* heterodimerization was investigated by immunoprecipitation of endogenous 14-3-3σ in U2OS cells and the results compared with those obtained by immunoprecipitating 14-3-3β. Samples were analyzed by two-dimensional gel electrophoresis and Western blotting to maximize resolution between individual isotypes. As shown in Fig. 2*A*, 14-3-3β was easily detectable in anti-β immunoprecipitates (*panel a*); however, no 14-3-3σ was pulled down in these samples (*panel b*). In contrast, a monoclonal antibody against 14-3-3σ strongly immunoprecipitated 14-3-3σ (*panel e*) but failed to immunoprecipitate any 14-3-3β (*panel d*). These data suggest that endogenous 14-3-3σ and β do not form mixed heterodimers. When the anti-β immunoprecipitates were blotted with an antibody that recognizes all of the 14-3-3 isotypes, at least 10 distinct spots were observed (*panel c*), consistent with extensive heterodimerization between β and

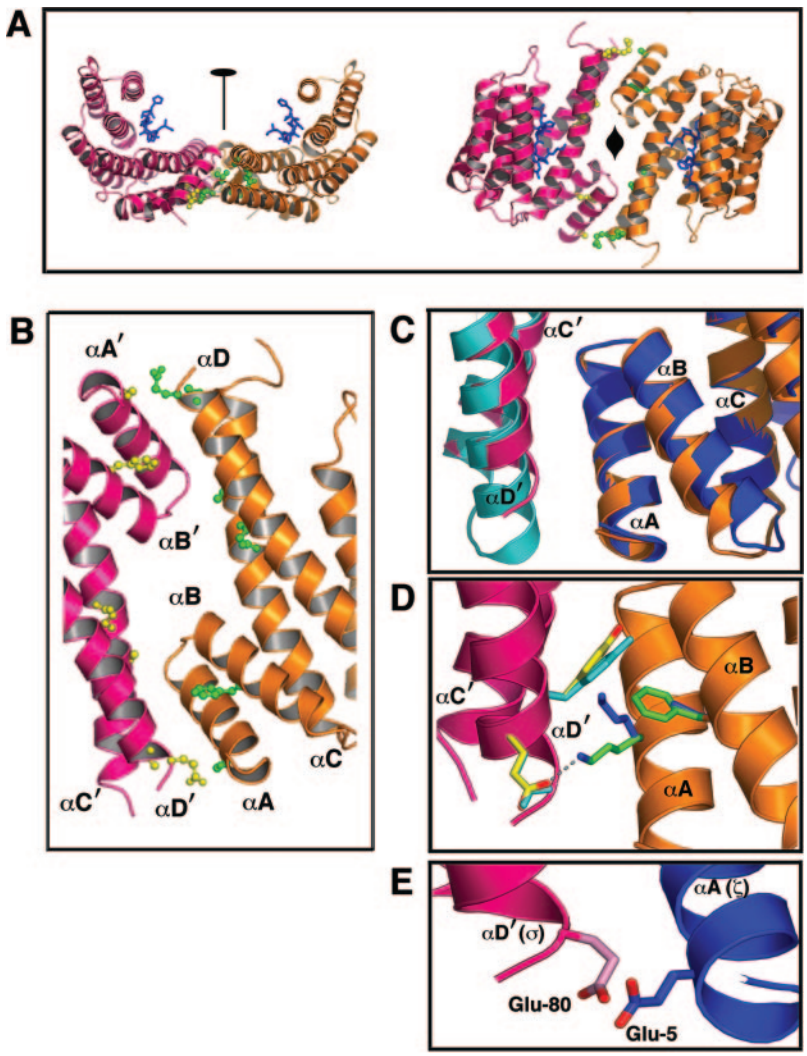

FIG. 3. **The structure of 14-3-3σ and the basis for homodimerization.** *A*, overview of the 14-3-3σ-mode-1 phosphopeptide complex. Two orthogonal views are shown with the protein in ribbons representation with one monomer colored *orange* and the other colored *pink*. The dimer 2-fold axis is indicated in each view. Side chains on either side of the interface that differ between the ζ and σ isoforms are shown as *yellow* and *green ball-and-stick* representations. The phosphopeptide, shown in *stick* representation, is colored *blue*. *B–E*, differences between the dimer interfaces of 14-3-3σ and -ζ facilitate homodimerization of the σ isoform. *B*, a close-up bottom view of the σ dimer rotated 180° from the view in the *right panel* of *A*, highlighting sequence differences at the interface. *C*, alignment of the structures of the σ and ζ isoforms reveals subtle differences in helix packing and register at the interface. The 14-3-3σ ribbon is colored as described for *A–C*, and the two monomers of the ζ isoform are colored *cyan* and *blue*, respectively. Sequence differences in the loop linking helices αB and αC (*orange*/*blue*) may be responsible for the different orientations of helix B. On the opposite side of the interface, 14-3-3σ is disordered in the loop connecting helices αC′ and αD′ (*pink*/*cyan*) where there is a two-amino acid insertion relative to the ζ sequence, and the αD′ helix has one less turn at its NH_2-terminal end. *D*, at the 14-3-3σ dimer interface a substitution of Phe (σ) for Cys (ζ) at residue 25 produces a ring-ring interaction between Phe-25 (αB) and Tyr-84 (αD′). The aromatic ring of Phe-25 prevents the alkyl chain of Lys-9 (αA) from participating in van der Waals interactions with Tyr-84 as seen at the ζ interface. Instead, Lys-9 makes a salt bridge across the interface with the side chain of Glu-83 at the end of the ordered part of helix αD′. *E*, in a modeled structure of the 14-3-3σ/ζ heterodimer interface, Glu-80 in 14-3-3σ αD′ (*pink*) would be juxtaposed against Glu-5 in αA of 14-3-3ζ (*blue*). This destabilizing interaction would similarly disrupt heterodimerization of σ with the β, ϵ, and τ isoforms as well.

other 14-3-3 isotypes. In contrast, when the anti-σ immunoprecipitates were probed with this same antibody (*panel f*), there were very few additional spots seen. These data indicate that 14-3-3σ preferentially forms homodimers within cells.

The specificity of the antibodies used in Fig. 2*A* is shown in Fig. 2*B*. To verify that the lack of 14-3-3σ heterodimerization we observed was not an artifact of dimer disruption by the anti-σ antibody, we transfected cells with a 2×FLAG-tagged 14-3-3σ construct and looked at its co-association with endogenous σ and β in anti-FLAG immunoprecipitates. As shown in Fig. 2*C*, endogenous 14-3-3σ dimerized with the 2×FLAG-tagged σ, while endogenous 14-3-3β did not. These findings confirm the conclusion, drawn from our two-dimensional gel results, that 14-3-3σ preferentially forms homodimers.

To understand the basis of preferential homodimerizaton, and to shed light on mechanisms of functional specificity for 14-3-3σ, we solved the x-ray crystal structure of 14-3-3σ bound to the mode-1 phosphopeptide MARSHpSYPAKKK at 2.4 Å resolution (Table I). As shown in Fig. 3*A*, the general shape of 14-3-3σ is essentially identical to that of 14-3-3τ and -ζ (34, 35), consisting of nine antiparallel α-helices forming a horseshoe-shaped dimer. The basis for dimer formation in 14-3-3σ is essentially the same as that of these other isotypes and involves a series of distributed interactions from residues in helices αA and αB in one monomer with residues in helices αC′ and αD′ in the other (Figs. 1*A* and 3*B*).

For simplicity, we focus further comparisons of the 14-3-3σ structure to that of 14-3-3ζ bound to the same mode-1 phosphopeptide (12), although the conclusions apply equally to those obtained by comparing 14-3-3σ with the unliganded

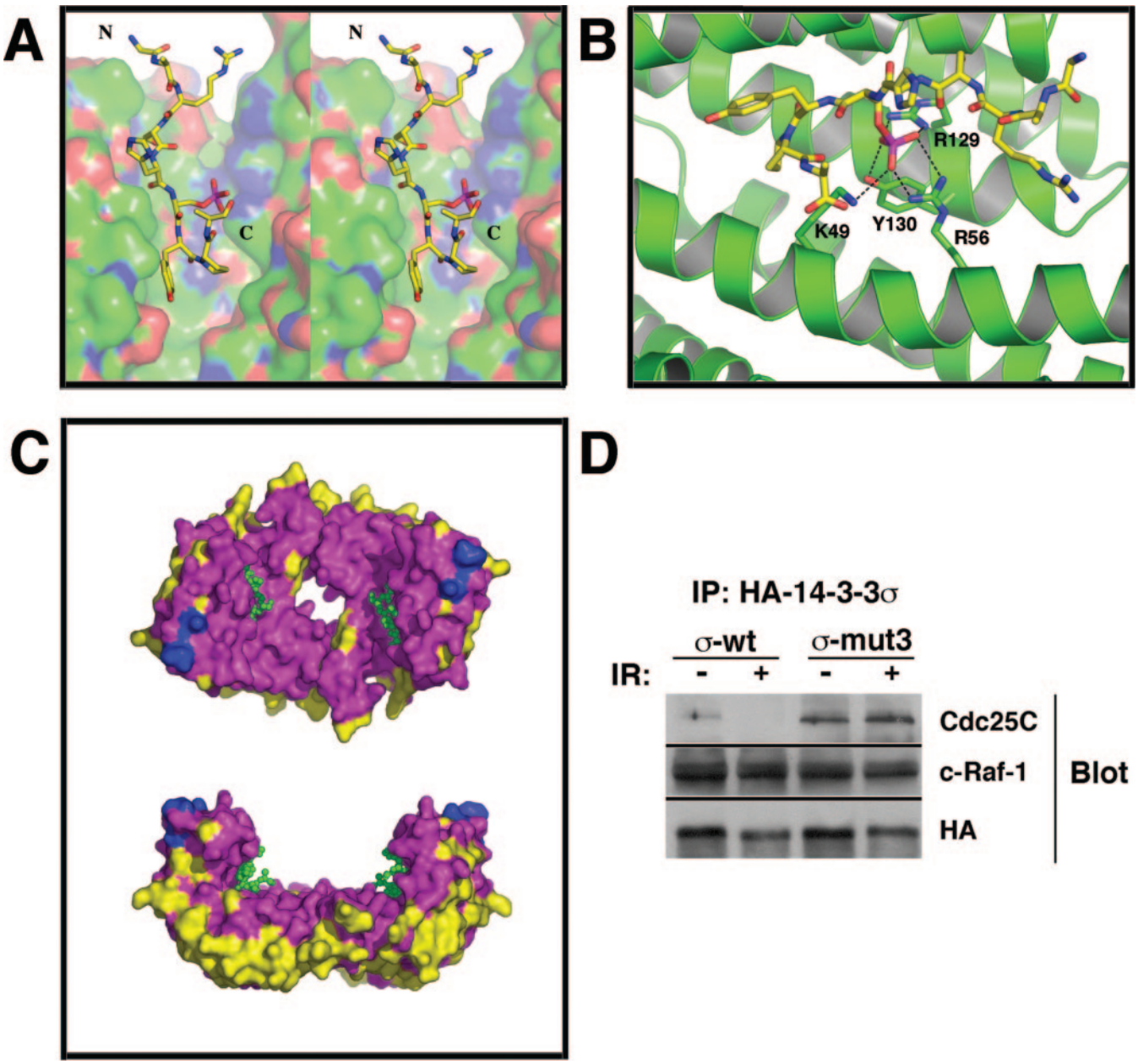

FIG. 4. **Ligand recognition by 14-3-3σ.** *A*, the phosphopeptide-binding pocket. Stereo view of the mode-1 phosphopeptide bound to one monomeric subunit of the 14-3-3σ dimer. The phosphopeptide is shown in stick representation with carbon atoms colored *yellow*, nitrogens *blue*, oxygens *red*, and phosphorus *purple*. 14-3-3σ is shown in surface representation shaded by similar atom-type color coding except with carbon colored *green*. *B*, molecular basis for phosphospecificity. The phosphate group of the phosphoserine is coordinated by four conserved 14-3-3 side chains. The protein backbone is represented by *green ribbons*; the phosphopeptide and the side chains that interact with the phosphate group are shown in *stick* representation. Key interactions observed between the phosphopeptide and 14-3-3σ are the same as those in the crystal structure of the 14-3-3ζ-phosphopeptide complex (12). *C*, a novel binding surface unique to 14-3-3σ. Surface representations of the 14-3-3σ dimer are shown along with a *ball-and-stick* representation of the phosphopeptide (*green*) in the same orientations as in Fig. 3*A*. The surfaces are color coded by sequence conservation with highly conserved residues shaded *magenta* and non-conserved residues *yellow*. Three exposed residues of 14-3-3σ (Met-202, Asp-204, and His-206), which differ from the absolutely conserved sequence in all other known isoforms, are shaded *blue*. These highly exposed residues protrude from the top of a prominent ridge above the concave face that contains the phosphopeptide-binding grooves. *D*, mutation of the novel binding surface of 14-3-3σ allows CDC25C ligand binding. U2OS cells were transfected with HA-14-3-3σ wild-type (*wt*) or a 14-3-3σ Met-202 → Ile,Asp-204 → Glu,His-206 → Asp triple mutant (*mut3*). 24 h following transfection, cells were irradiated (*IR*) with 10 grays of ionizing radiation or received no treatment, and were lysed 4 h later. Whole cell lysates were immunoprecipitated (*IP*) with an anti-HA antibody, separated by SDS-PAGE, and blotted with antibodies against Cdc25C (*upper panel*), c-Raf-1 (*middle panel*), and the HA epitope (*lower panel*).

structure of 14-3-3τ (34). In 14-3-3σ the angle between αA and αB is different from that in the ζ dimer. This difference may be related to the unique sequence of the BC loop in 14-3-3σ compared with that in other human isoforms. Across the dimer interface in the opposing monomer, the loop connecting helices αC′ and αD′, which contains two extra amino acids in 14-3-3σ, is disordered and helix αD′ is one turn shorter at its amino-terminal end than in the 14-3-3ζ structure. Helices αA and αD′ in the 14-3-3σ structure are observed to pack slightly closer together across the interface than in ζ (Fig. 3*C*), perhaps as a consequence of these changes.

There are seven amino acid differences between 14-3-3σ and 14-3-3ζ at the dimer interface (six between σ and τ). Five of these amino acid substitutions are σ-specific and must provide a structural basis for σ homodimerization through stabilizing homodimeric interactions and destabilizing heterodimeric in-

teractions. In the 14-3-3σ structure, Phe-25, which is unique to σ, makes a ring-ring interaction across the interface with Tyr-84 on αD′ (Fig. 3*D*). The aromatic ring of the Phe-25 side chain prevents Lys-9 (on αA) from adopting the conformation it has in the 14-3-3ζ structure. Instead, in the 14-3-3σ structure Lys-9 participates in a salt bridge with Glu-83 located at the NH_2-terminal end of αD′. Because of 2-fold symmetry, these σ-specific ring-ring and salt-bridge interactions occur twice in the dimer. Thus, the 14-3-3σ homodimer has four stabilizing interactions that cannot occur in heterodimers that include 14-3-3σ.

Furthermore, Ser-5 and Glu-80, both unique to 14-3-3σ (Fig. 1*A*), lie opposite each other at the dimer interface (Fig. 3*B*), near the disordered NH_2 terminus of αD of 14-3-3σ. In 14-3-3σ-containing heterodimers with the τ, ζ, β, or ϵ isoforms, Glu-80 in σ would be in close proximity to the Asp or Glu side chain that replaces Ser-5 of σ (Fig. 3*E*), resulting in a highly unfavorable interaction between these two opposing negative charges. Thus, in addition to the loss of the two stabilizing homodimeric interactions mentioned above, heterodimers of 14-3-3σ with these isoforms would be required to tolerate an additional highly destabilizing interaction across the dimer interface. Furthermore, favorable packing of the bulky hydrophobic Met or Leu sidechains corresponding to Glu-80 in the ϵ, β, ζ, τ, and γ isoforms may be incompatible with the subtle shifts in the positions of αA and αB in 14-3-3σ. Taken together, these observations suggest a structural basis for our results showing that the σ isoform preferentially forms homodimers.

Each of the C2 symmetry related monomers of the 14-3-3σ dimer contains a phosphopeptide binding pocket running in opposite directions, in which residues 5–10 of the peptide (Ser-His-Ser(P)-Tyr-Pro-Ala) are clearly visible. On one side, poor but interpretable density is present for residues 2–4 (Gly-Ala-Arg). The conformation of the bound phosphopeptide is essentially the same as that in the corresponding complex with 14-3-3ζ. For each monomer, the peptide binds in a narrow cleft formed primarily by the surface-exposed residues from αA,αB, αC, and αD on the concave surface of the molecule (Fig. 4*A*). The topography of the cleft requires that the peptide have a distinct kink that allows it to exit the channel after which it becomes disordered in the structure. This kink is produced by a cis-Pro residue in the +2 position. The details of the interaction between the protein and the phosphopeptide are the same as in the 14-3-3ζ-mode1 peptide complex. All of the key interactions, including those involved in coordinating the phosphate group of the phosphoserine (Fig. 4*B*), are essentially identical. This is not surprising, as the sequence identity of the residues that comprise the phosphopeptide-binding site are strictly conserved (Fig. 4*C*). Consequently, the selectivity of 14-3-3σ selectivity for specific ligands must involve other sites besides the major phosphopeptide-binding groove.

Most of the non-conserved residues are exposed on the opposite face of the dimer from the concave depression that contains the phosphopeptide binding site. However, a patch of three residues in the αH-αI linker (Met-202, Asp-204, and His-206), strictly conserved in every sequence in Fig. 1*A* except 14-3-3σ, is exposed at the extreme ends of the ridges at the tops of either side of the U-shaped dimer. These three residues form a small island of exposed non-conserved sequence surrounded mostly by conserved sequence (Fig. 4*C*). This observation suggests that this site might constitute a 14-3-3σ-specific binding site for other protein ligands. Intriguingly, the patch formed by these three residues lies adjacent to the invariant Phe-198 (position 204 in the alignment in Fig. 1*A*), whose mutation in the *Drosophila* epsilon isoform appears to impair Raf/14-3-3 interactions required for Ras-mediated signaling (36). In addition, the αH-αI linker in 14-3-3ζ makes direct contact with part of serotonin *N*-acetyltransferase in the 14-3-3ζ-AANAT co-crystal structure (37). These findings further suggest that this region of 14-3-3σ may indeed be part of a second ligand binding surface.

To investigate this, and determine whether this site was involved in σ-specific ligand discrimination, we mutated Met-202, Asp-204, and His-206 in σ to the Ile, Glu, and Asp residues that are present in all other non-σ isotypes and transfected the resulting HA-tagged construct into U2OS cells (Fig. 4*D*). Both wild-type and the triple mutant σ bound to c-Raf-1 in cells. In contrast, wild-type σ did not bind significantly to Cdc25C, whereas the triple mutant form of σ showed robust binding, as well as a slight increase in Cdc25C binding after irradiation-induced DNA damage, particularly when normalized to the amount of HA-14-3-3σ in the IPs. These findings strongly suggest that this region in 14-3-3σ normally constitutes a second phospho-independent ligand-binding site that is likely to be involved in mediating selection for and against specific ligands. Similar phospho-independent ligand-binding surfaces that are spatially separate from the phosphopeptide-binding pocket have also been observed in other phosphoserine/threonine-binding domains (38).

In conclusion, we have shown that endogenous 14-3-3σ preferentially forms homodimers in cells, a finding that can be rationalized at the structural level by sequence differences and selective interactions at the dimer interface. The structural basis of 14-3-3σ phosphopeptide-binding is essentially identical to that seen in 14-3-3ζ phosphopeptide and protein complexes (12, 37, 39), suggesting that 14-3-3σ-specific substrate discrimination involves alternative secondary surfaces. We have identified one of these surfaces in the αH-αI linker involving residues Met-202, Asp-204, and His-206. Mutation of this σ-specific surface patch to the corresponding sequence in other 14-3-3 proteins causes 14-3-3σ to bind to Cdc25C, a molecule that normally binds to other 14-3-3 isoforms but not to σ. These findings may assist in understanding the molecular basis for 14-3-3σ-specific function in cell cycle control and cancer.

Acknowledgments—We gratefully acknowledge the technical assistance from Yun Feng and Daniel Lim, Drew M. Lowery for the construction of pCDNA3.1+2X Flag, and the editorial assistance of Stephen J. Smerdon. This work was conducted at the Northeastern Collaborative Access Team beamlines of the Advanced Photon Source, which is supported by award RR-15301 from the National Center for Research resources at the National Institutes of Health.

REFERENCES

1. Aitken, A. (1996) *Trends Cell Biol.* **6,** 341–347
2. Fu, H., Subramanian, R. R., and Masters, S. C. (2000) *Annu. Rev. Pharmacol. Toxicol.* **40,** 617–647
3. Tzivion, G., Shen, Y. H., and Zhu, J. (2001) *Oncogene* **20,** 6331–6338
4. van Hemert, M. J., Steensma, H. Y., and van Heusden, G. P. (2001) *BioEssays* **23,** 936–946
5. Wilker, E., and Yaffe, M. B. (2004) *J. Mol. Cell. Cardiol.* **37,** 633–642
6. Aitken, A., Howell, S., Jones, D., Madrazo, J., and Patel, Y. (1995) *J. Biol. Chem.* **270,** 5706–5709
7. Dubois, T., Rommel, C., Howell, S., Steinhussen, U., Soneji, Y., Morrice, N., Moelling, K., and Aitken, A. (1997) *J. Biol. Chem.* **272,** 28882–28888
8. Megidish, T., Cooper, J., Zhang, L., Fu, H., and Hakomori, S. (1998) *J. Biol. Chem.* **273,** 21834–21845
9. Powell, D. W., Rane, M. J., Joughin, B. A., Kalmukova, R., Hong, J. H., Tidor, B., Dean, W. L., Pierce, W. M., Klein, J. B., Yaffe, M. B., and McLeish, K. R. (2003) *Mol. Cell. Biol.* **23,** 5376–5387
10. Jones, D. H., Ley, S., and Aitken, A. (1995) *FEBS Lett.* **368,** 55–58
11. Chaudhri, M., Scarabel, M., and Aitken, A. (2003) *Biochem. Biophys. Res. Commun.* **300,** 679–685
12. Yaffe, M. B., Rittinger, K., Volinia, S., Caron, P. R., Aitken, A., Leffers, H., Gamblin, S. J., Smerdon, S. J., and Cantley, L. C. (1997) *Cell* **91,** 961–971
13. Nguyen, A., Rothman, D. M., Stehn, J., Imperiali, B., and Yaffe, M. B. (2004) *Nat. Biotechnol.* **22,** 993–1000
14. Manke, I. A., Nguyen, A., Lim, D., Stewart, M. Q., Elia, A. E., and Yaffe, M. B. (2005) *Mol. Cell* **17,** 37–48
15. Hermeking, H., Lengauer, C., Polyak, K., He, T. C., Zhang, L., Thiagalingam, S., Kinzler, K. W., and Vogelstein, B. (1997) *Mol. Cell* **1,** 3–11
16. Chan, T. A., Hermeking, H., Lengauer, C., Kinzler, K. W., and Vogelstein, B. (1999) *Nature* **401,** 616–620

17. Peng, C. Y., Graves, P. R., Thoma, R. S., Wu, Z., Shaw, A. S., and Piwnica-Worms, H. (1997) *Science* **277,** 1501–1505
18. Kumagai, A., Yakowec, P. S., and Dunphy, W. G. (1998) *Mol. Biol. Cell* **9,** 345–354
19. Dalal, S. N., Schweitzer, C. M., Gan, J., and DeCaprio, J. A. (1999) *Mol. Cell. Biol.* **19,** 4465–4479
20. Donzelli, M., and Draetta, G. F. (2003) *EMBO Rep.* **4,** 671–677
21. Dalal, S. N., Yaffe, M. B., and DeCaprio, J. A. (2004) *Cell Cycle* **3,** 672–677
22. Vercoutter-Edouart, A. S., Lemoine, J., Le Bourhis, X., Louis, H., Boilly, B., Nurcombe, V., Revillion, F., Peyrat, J. P., and Hondermarck, H. (2001) *Cancer Res.* **61,** 76–80
23. Ferguson, A. T., Evron, E., Umbricht, C. B., Pandita, T. K., Chan, T. A., Hermeking, H., Marks, J. R., Lambers, A. R., Futreal, P. A., Stampfer, M. R., and Sukumar, S. (2000) *Proc. Natl. Acad. Sci. U. S. A.* **97,** 6049–6054
24. Iwata, N., Yamamoto, H., Sasaki, S., Itoh, F., Suzuki, H., Kikuchi, T., Kaneto, H., Iku, S., Ozeki, I., Karino, Y., Satoh, T., Toyota, J., Satoh, M., Endo, T., and Imai, K. (2000) *Oncogene* **19,** 5298–5302
25. Suzuki, H., Itoh, F., Toyota, M., Kikuchi, T., Kakiuchi, H., and Imai, K. (2000) *Cancer Res.* **60,** 4353–4357
26. Umbricht, C. B., Evron, E., Gabrielson, E., Ferguson, A., Marks, J., and Sukumar, S. (2001) *Oncogene* **20,** 3348–3353
27. Urano, T., Saito, T., Tsukui, T., Fujita, M., Hosoi, T., Muramatsu, M., Ouchi, Y., and Inoue, S. (2002) *Nature* **417,** 871–875
28. Dellambra, E., Golisano, O., Bondanza, S., Siviero, E., Lacal, P., Molinari, M., D'Atri, S., and De Luca, M. (2000) *J. Cell Biol.* **149,** 1117–1130
29. Brunet, A., Kanai, F., Stehn, J., Xu, J., Sarbassova, D., Frangioni, J. V., Dalal, S. N., DeCaprio, J. A., Greenberg, M. E., and Yaffe, M. B. (2002) *J. Cell Biol.* **156,** 817–828
30. Otwinowski, Z. (1993) in *Data Collection and Processing* (Sawyers, L., Isaacs, N., and Bailey, S., eds) pp. 56–62, SERC Daresbury Laboratory, Warrington, UK
31. CCP4 (1994) *Acta Crystallogr. Sect. Sect. D Biol. Crystallogr.* **50,** 760–763
32. Brunger, A. T., Adams, P. D., Clore, G. M., DeLano, W. L., Gros, P., Grosse-Kunstleve, R. W., Jiang, J. S., Kuszewski, J., Nilges, M., Pannu, N. S., Read, R. J., Rice, L. M., Simonson, T., and Warren, G. L. (1998) *Acta Crystallogr. Sect. D Biol. Crystallogr.* **54,** 905–921
33. Jones, T. A., Zou, J. Y., Cowan, S. W., and Kjeldgaard. (1991) *Acta Crystallogr. Sect. A* **47,** 110–119
34. Xiao, B., Smerdon, S. J., Jones, D. H., Dodson, G. G., Soneji, Y., Aitken, A., and Gamblin, S. J. (1995) *Nature* **376,** 188–191
35. Liu, D., Bienkowska, J., Petosa, C., Collier, R. J., Fu, H., and Liddington, R. (1995) *Nature* **376,** 191–194
36. Chang, H. C., and Rubin, G. M. (1997) *Genes Dev.* **11,** 1132–1139
37. Obsil, T., Ghirlando, R., Klein, D. C., Ganguly, S., and Dyda, F. (2001) *Cell* **105,** 257–267
38. Li, J., Williams, B. L., Haire, L. F., Goldberg, M., Wilker, E., Durocher, D., Yaffe, M. B., Jackson, S. P., and Smerdon, S. J. (2002) *Mol. Cell* **9,** 1045–1054
39. Rittinger, K., Budman, J., Xu, J., Volinia, S., Cantley, L. C., Smerdon, S. J., Gamblin, S. J., and Yaffe, M. B. (1999) *Mol. Cell* **4,** 153–166
40. Felsenstein, J. (1989) *Cladistics* **5,** 164–166